Meccanica (2020) 55:2285–2304
https://doi.org/10.1007/s11012-020-01248-5

Stress analysis of strain wave gear drives with four different geometries of wave generator

Eloy Yague-Spaude · Ignacio Gonzalez-Perez · Alfonso Fuentes-Aznar

Received: 14 May 2020 / Accepted: 19 September 2020 / Published online: 15 October 2020

Abstract The comparison of strain wave gear drives with four different geometries of the wave generator is presented. The commonly used elliptical geometry of the wave generator is compared with a simplified geometry based on two rolling elements, a geometry based on four rollers, and a newly proposed parabolic geometry for the wave generator. The comparison will be performed in terms of the average maximum stresses caused in the flexible spline due to the rotation of the wave generator. The finite element method and fully-parameterized automatically-generated two-dimensional finite element models are being used in this work. The flexible spline and the ring gear are considered deformable elements whereas the wave generator is considered as a rigid element in the finite element model. The results show that the best mechanical performance in terms of lower average values of maximum von Mises and tensile stresses is achieved with the simplified and parabolic wave generator geometries. Although yielding slightly higher maximum von Mises and tensile stresses, the elliptical wave generator provides the lowest average maximum absolute compressive stress. The worst mechanical performance was obtained with the four roller wave generator.

Keywords Strain wave gears · Wave generator geometry · Stress analysis · Finite element method

E. Yague-Spaude · A. Fuentes-Aznar (✉)
Department of Mechanical Engineering, Kate Gleason College of Engineering, Rochester Institute of Technology, Rochester, NY 14623, USA
e-mail: afeme@rit.edu

E. Yague-Spaude
e-mail: ey6232@rit.edu

I. Gonzalez-Perez
Department of Mechanical Engineering, Materials and Manufacturing, Polytechnic University of Cartagena, 30202 Cartagena, Spain
e-mail: ignacio.gonzalez@upct.es

1 Introduction

Since their invention in 1959 by Clarence Walton Musser [1], SWG drives have been applied in many applications in the fields of motion control and machine tools. Recently, they have been widely applied in robotics and aerospace. They provide a large gear reduction ratio in a remarkably reduced, compact, and lightweight construction as compared to traditional gear drives. Besides, SWG drives can work with virtually no backlash. This is considerably helpful in robotic joints as well as in aerospace and other applications where space and weight are critical constrains.

A SWG drive consists of three main components: a wave generator, a flexible spline, and a ring gear, as shown in Fig. 1. The wave generator is usually an

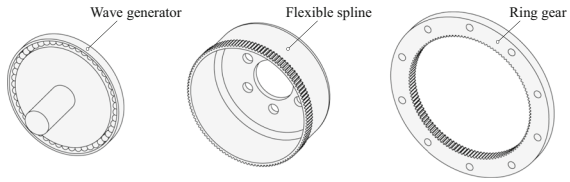

Fig. 1 Components of a SWG drive

elliptical cam with a flexible race ball bearing around its outer geometry. The flexible spline is a cup-shaped spring with an external teeth gear located on the open end of the cup while the ring gear is an internal teeth gear. Inserted in the flexible spline, the wave generator deforms the toothed region of the flexible spline into meshing with the internal teeth of the ring gear.

The number of teeth of the flexible spline and the ring gear differ in a multiple of the number of lobes of the wave generator. Due to the use of elliptical wave generators, the flexible spline is two teeth smaller than the ring gear [1]. Typically, the input member in SWG drives is the wave generator, which deforms the flexible spline into meshing with the ring gear. Figure 2 shows the most common layouts of SWG drives. In Fig. 2a, the closed end of the cup of the flexible spline provides the output from the drive while the ring gear is fixed. On the other hand, Fig. 2b shows the layout where the flexible spline is fixed and the ring gear serves as output.

In order to study the behavior of SWG drives, researchers have developed kinematic and dynamic models receiving input deflection and torque information from strain gauges on the flexible spline [2]. In [3], the authors aimed to develop the simplest possible model to represent and correct the torque transmission non-linearities in SWG drives. They realized that stiffness and damping of the flexible spline are critical parameters toward representing the behavior of SWG drives.

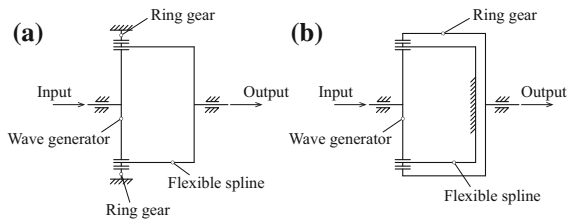

Fig. 2 Typical layouts and transmission of motion in SWG drives

More recently, in [4] a dynamic model was proposed considering the drive as a grey box calibrated by non-linear regression means. However, the model was considerably simplified by averaging the contact between engaged tooth pairs. A built-in torque sensor was used in [5] to develop a dynamic model to compensate torque ripples in SWG drives.

Regarding the use of finite element analysis, several authors have also proposed its application on SWG drives. In [6], finite element analysis is used to develop a suitable tooth profile for the flexible spline and the ring gear, while in [7], stress analysis is performed to identify how the flexible spline behaves with fatigue loads. Finite element analysis was used to evaluate the influence of the shape of the wave generator and the transmitted load over stresses in [8]. The authors realized that the deformations of the flexible spline are heavily non-linear, which makes understanding the behavior of SWG drives a required application of finite element analysis.

In [9], a two-dimensional finite element model was used to evaluate the influence of torque and pressure angle over torsional stiffness, the number of teeth in contact, and stresses in SWG drives. These analyses were performed with the wave generator and the ring gear fixed while applying torque to the flexible spline. The selected tooth profile was the involute tooth profile, also studied in [10] and [11], where the authors performed several studies using finite element analysis on SWG drives to conclude that there are several pairs of teeth in contact as a function of the load applied and the geometry of the wave generator employed.

In [12], simulation of meshing of SWG drives was performed and the obtained results were verified with experiments and finite element analysis. The authors studied the variation of meshing stiffness and number of teeth in contact as a function of time and torque applied. Finally, in [13], several geometries of the wave generator are evaluated with a considerably simplified finite element model. A more realistic finite element model of SWG drives was developed in [14]. The aim was to compute circumferential stresses on the flexible spline as a function of the length of the cup and compare them to a rapid analytical method developed by the authors. The results, however, are not considerably accurate.

Several different geometries of the wave generator in SWG drives have been proposed over time. Musser [1] proposed the application of an elliptical wave

generator in his patent. In [15, 16], a wave generator based on two connected circular arcs, that resemble two circular rollers, was proposed and applied. In [17], a wave generator comprising of four rollers was patented.

This paper displays a comparison of the stresses developed in the flexible spline by different geometries of the wave generator. Additionally, a wave generator of parabolic geometry will be studied and compared with existing types of geometries. The same tooth profiles of the flexible spline and ring gear will be maintained regardless of the geometry of the wave generator being investigated. The stress analysis will be based on two-dimensional finite element models that consider the outer geometry of the wave generator as a rigid element as well as the geometry of the rim and teeth of both the flexible spline and the ring gear as deformable elements. The two-dimensional finite element model includes the load transmitted by the drive and simulates the meshing of SWG drives by rotating the wave generator as input member. Different analyses will be performed as a function of the various design parameters of the wave generator to determine their improved design and relative comparison of their mechanical performance in terms of maximum stresses throughout the meshing process.

2 Description of the finite element model

The applied finite element model considers a planar slice of the different elements of a SWG drive. This includes the tooth geometry and rim region of both the flexible spline and the ring gear as deformable elements. However, due to the continuously imposed deflection on the flexible spline by the wave generator, the geometry of the latter is considered rigid in this study.

Figure 3 shows the different parts included in the finite element model on the global coordinate system S at the initial stage of the analysis. The points labelled RP_i (i = pp, wg, fs, rg) are the reference nodes of the different parts, where subscripts "pp", "wg", "fs", and "rg" refer to the pushing pins, wave generator, flexible spline, and ring gear, respectively. This figure does not show the reference nodes of the flexible spline RP_{fs} and the ring gear RP_{rg} because they coincide with the reference node of the wave generator

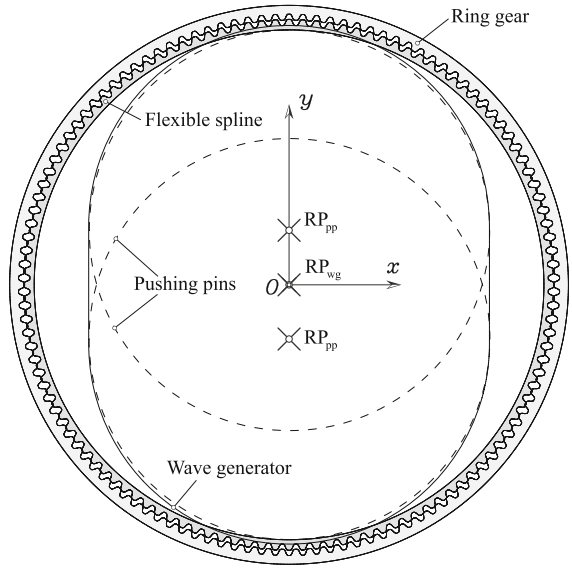

Fig. 3 Assembled parts of the two dimensional finite element model at the initial stage before deflection is imposed

RP_{wg}. The flexible spline is not deflected at the beginning of the analysis and interferes with the ring gear, as shown in Fig. 3. Since the lobes or major axis regions of the wave generator incorporate the to-be-imposed deflection on the flexible spline, the lobes also interfere with the undeformed flexible spline at the initial stage.

The pushing pins are artifacts used to set-up the finite element model before the simulation of meshing begins. The pushing pins resemble the regions or lobes of the wave generator that will be in contact with the inner diameter of the flexible spline during the meshing process. These pins are used only at the beginning of the analysis to deflect the flexible spline into contact with the ring gear and deactivated later once the pushing pins are replaced by the actual geometry of the wave generator.

The finite element meshes of the flexible spline and the ring gear are obtained automatically, fully parameterized by a virtual gear generator computer program. In such, the number of elements of each section of the tooth geometry of the deformable parts are selected, as shown in Fig. 4. The tooth geometry is divided in five sections where the number of elements are specified (top land and active profiles, upper rim, lower rim, and inner/outer diameter). The number of elements under the top land profile coincides with those in the upper

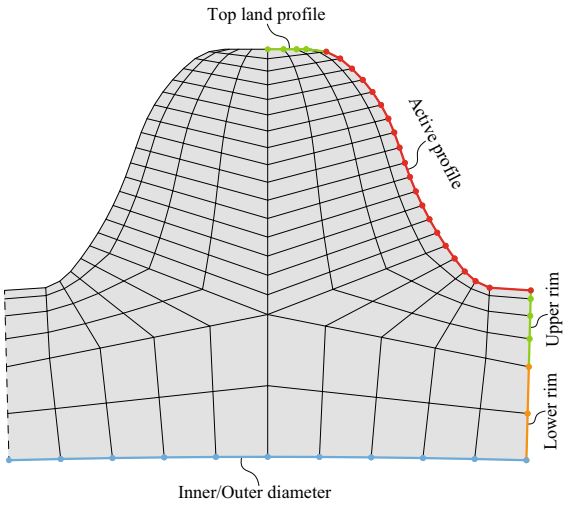

Fig. 4 Two-dimensional parameterized finite element mesh on a flexible spline or ring gear tooth

rim. The inner and the outer diameters are defined for the flexible spline and the ring gear, respectively.

Several analyses have been performed varying the number of elements in each section to set up the mesh size for this study. Their variation only leads to small changes in resulting stresses on the two-dimensional model. Since each model to be compared uses the same mesh size, numerical errors due to the finite element mesh size are cancelled out when comparing level of stresses among different models. Table 1 shows the different element types used in the finite element model, their characteristics, and the number of nodes and elements of each part. These elements will be further illustrated in Fig. 8. Finite elements of type CPS4I consisting of plane stress bilinear elements with four nodes and incompatible modes to improve their bending behavior [18] have been applied to the flexible spline (fs) and the ring gear (rg). The wave generator (wg) and pushing pins (pp) for the selected wave generator are considered as rigid and meshed with R2D2 elements, which are two-dimensional linear rigid elements with two nodes connected by a linear link and designed for plane strain or plain stress analyses [18]. For this reason, the meshes of both the wave generator and the pushing pins are defined by linear elements coinciding with their outer geometry, as shown in Fig. 3. The deformable geometries of flexible spline and ring gear whose teeth are meshed according to Fig. 4 implement the vast majority of nodes and elements in the model. On the other hand, the rigid linear geometries of the wave generator and the pushing pins require considerably less nodes and elements. The elements of each of the parts are connected to a reference node (*RP*) and all their degrees of freedom are related to the movement of their reference node. This means that the required boundary conditions to represent the behavior of SWG drives throughout the simulation of meshing are applied on the reference nodes *RP* of each element.

2.1 Set-up steps for finite element analysis

The finite element model includes several steps to organize the engagement and disengagement of its different contact interactions, as well as the application of boundary conditions and loads. As an example, Fig. 5 shows the variations of maximum tensile stress (maximum principal stress σ_1), the absolute maximum compressive stress (minimum principal stress $|\sigma_3|$), and the equivalent von Mises stress (σ) on the flexible spline throughout an entire analysis for one of the cases of design that later will be presented in detail. A full analysis consists of the required set-up steps for the deflection of the flexible spline into contact with the ring gear (Step -2), engagement of the wave

Table 1 Parameters of the finite element mesh

Element type	Properties	Characteristic	Number of nodes	Usage
CPS4I	Plane stress	Bilinear	4	fs, rg
R2D2	Rigid	Linear	2	pp, wg
	Mesh size			
	fs	rg	pp	wg
Number of nodes	26,161	26,597	200 × 2	599
Number of elements	22,560	22,936	199 × 2	598

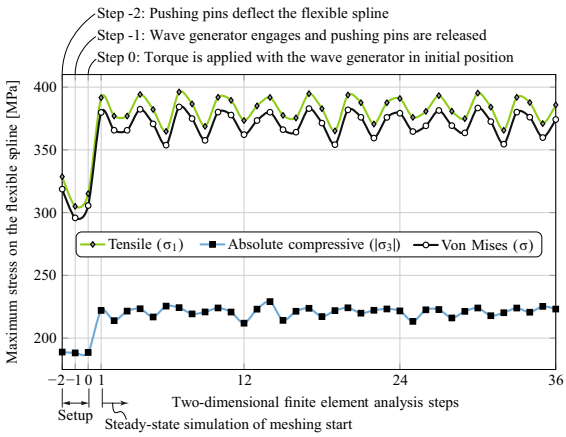

Fig. 5 Variation of maximum tensile stress on the flexible spline throughout the steps of the finite element analysis

generator with the flexible spline (Step -1), application of the transmitted load (Step 0), and simulation of the process of meshing by rotating the wave generator a half revolution or more (steps 1 to end). The horizontal axis in Fig. 5 shows the different steps included in the finite element model. During Step -2, the pushing pins impose the required deflection on the flexible spline. This brings the teeth of the flexible spline into meshing with those of the ring gear in Step -1. The maximum stresses remain low until the transmitted load is applied in Step 0 which finishes the setup of the model for simulation of meshing of SWG drives.

Figure 5 shows the variations of maximum stresses on the flexible spline where the largest stress is the tensile stress (σ_1) and the lowest is the absolute compressive ($|\sigma_3|$). The maximum equivalent von Mises stress (σ) is similar to the tensile stress, although slightly lower due to the influence of the compressive stress. In this work, the average value of the maximum von Mises stress on the flexible spline throughout the different steps of the analysis corresponding to half revolution of the wave generation will be used for comparison of the mechanical behavior.

Figure 6 shows the different parts included in the finite element model after the deflection has been applied to the flexible spline by the pushing pins in Step -2. Notice that the location of the pushing pins after applying the deflection to the flexible spline recreates the geometry of the wave generator. This allows the deactivation of the pushing pins and the engagement of the wave generator to continue with the

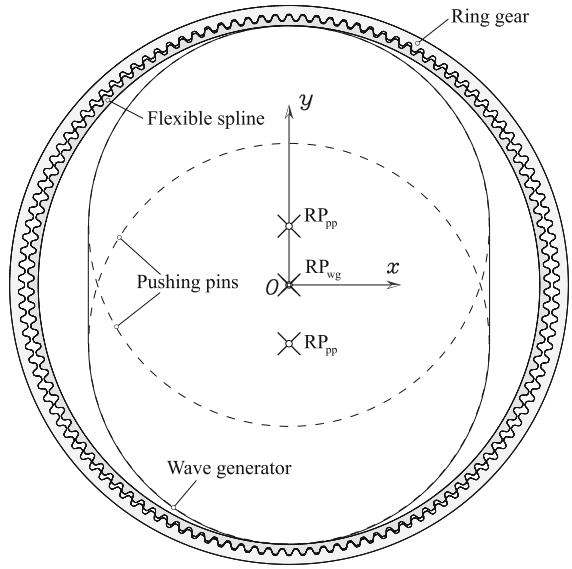

Fig. 6 Assembled parts of the two dimensional finite element model after deflection is imposed

deflection of the flexible spline during Step -1. Then, in Step 0 and with the wave generator in its initial position for the analysis, the torque is applied on the output element of the drive (the flexible spline or the ring gear) until reaching its full value by the end of this step. This torque can be modified to represent the actual non-linear output torque that SWG drives transmit [5, 19]. Once Step 0 is finished, the model is ready to continue with the simulation of the process of meshing when the wave generator rotates.

From Step 1 and on, the wave generator is rotated at each step in small increments until a half rotation of the wave generator is completed in order to perform a steady-state simulation of the process of meshing. The maximum tensile stress during the first two steps (-2 and -1) is considerably lower than that obtained during the simulation of meshing beyond Step 0 due to the progressive application of torque at Step 0 until reaching its full value at the end of Step 0. Then, from Step 1 onward, the torque is fully applied and maintained throughout the simulation of meshing.

Steps 0 and 1 are being considered for stress analysis, whereas Steps -2 and -1 are only considered to set up the model. Steps 0 and 1 serve to show the effect of the application of torque on the stresses at the beginning of the analysis, as well as the set-up for simulation of meshing. However, average stresses throughout the process of simulation of meshing are

computed taking into account the results from Step 1 until the end of the analysis after a half revolution of the wave generator.

2.1.1 *Influence of the rotation steps*

The simulation of meshing is performed by rotating the wave generator 180 degrees, divided in small incremental rotations depending of the number of steps considered for the analysis. At each step of rotation, the maximum stresses are computed. However, a wavy evolution of the stresses has been found and, depending on the considered number of steps of rotation, the sampling of the maximum stresses may lead to different evolutions of the maximum stresses as shown in Fig. 7. Figure 7 shows the variation of maximum von Mises stress on the flexible spline throughout the process of simulation of meshing for different numbers of steps dividing half a revolution of the wave generator as input member. The selected numbers of steps are 180, 60, and 36 resulting on increments of the rotation angle of the wave generator equal to 1, 3, and 5 degrees per step, respectively.

Depending on the number of steps and the increment of the rotation that each step performs, the maximum stresses on the flexible spline oscillate throughout the meshing. Combinations of steps where the 180 degrees of wave generator rotation are divided in multiples of 3 degrees per step do not show frequent oscillatory behavior throughout the simulation of meshing as shown in Fig. 7. These cases show a smooth curve that oscillates between a maximum and a minimum value of the evolution of the maximum

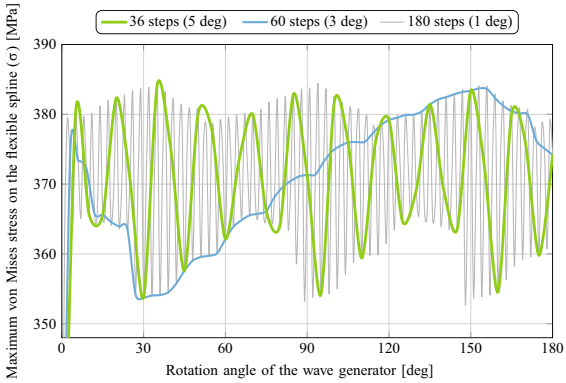

Fig. 7 Variation of maximum von Mises on the flexible spline throughout the simulation of meshing with different number of steps

von mises stress and repeats every half revolution of the wave generator. On the other hand, combinations of steps where half revolution of the wave generator is divided in a number of steps not leading to a multiple of 3 degrees per step show frequent, small, and repeated oscillations of the maximum von Mises stresses.

Regardless of the oscillatory behavior of the variations of maximum tensile, absolute compressive, and von Mises stresses, their ranges, as well as their average value remain constant regardless of the number of steps employed for the meshing simulation. For this reason, the results presented in this work will be obtained considering half a revolution of the wave generator divided in 36 steps of 5 degrees of rotation per step. The lower number of steps to compute stresses provides enough detail about the oscillating variation of the maximum stresses while requiring less computational effort.

2.2 Contact interactions and boundary conditions in the finite element model

The following three contact interactions are defined in the employed finite element model:

- Interaction of the pushing pins and inner diameter of the flexible spline.
- Interaction of the wave generator and inner diameter of the flexible spline.
- Interaction of the flexible spline tooth surfaces and the ring gear tooth surfaces.

These interactions are based on hard contact between surfaces [18]. The contact between the pushing pins and the flexible spline and between the wave generator and the flexible spline is considered frictionless. This is due to the use of a flexible race ball bearing around the wave generator which rotates with the flexible spline while the wave generator provides the input motion. On the other hand, the contact between the teeth of the flexible spline and the ring gear considers the presence of static friction between the teeth due to the low tooth sliding velocities in SWG drives [1].

The contact interactions, however, are not active throughout all the steps of the model due to the interference between the different parts at the initial stage. The contact interactions between the wave generator and the flexible spline and between the

flexible spline and the ring gear are activated in Step-1 to permit interference throughout the application of deflection in Step-2. From Step-1 until the end of the analysis, the only interactions occur as contact between the wave generator and the flexible spline and the teeth of the flexible spline and those of the ring gear, while the contact between the pushing pins and the flexible spline is deactivated. Figure 8 shows a section of the two-dimensional model once the setup for the simulation of meshing is completed. The contact interactions extend around the entire geometry of the affected elements to allow for further rotation of the wave generator for meshing simulation.

Considering the layout of SWG drives where the flexible spline is the output element and the ring gear is the fixed element, the outer geometry of the ring gear is fixed throughout the entire analysis while the torque is applied on the flexible spline reference node RP_{fs}. This node RP_{fs} is connected to the inner diameter of the flexible spline with a coupling which connects the degrees of freedom of this reference node RP_{fs} to the inner nodes of the flexible spline. This coupling transmits the output torque T to the entire circumference of the flexible spline throughout the process of simulation of meshing.

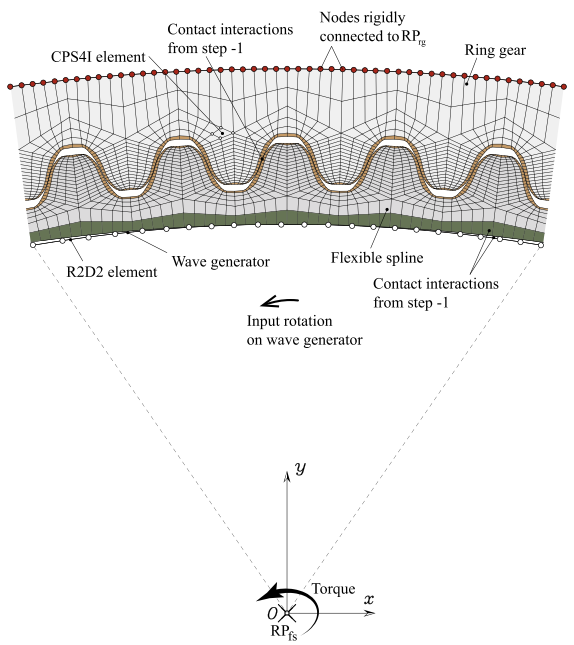

Fig. 8 Contact interactions between the different elements of SWG drives in the two-dimensional model

2.3 Applied gear tooth profile

A quadruple circular arc (QCA) tooth profile shown in Fig. 9 has been applied for the teeth of the flexible spline and the ring gear. The QCA profile is a directly defined tooth profile employing a combination of circular arcs and a straight segment for each flank of a tooth of the flexible spline and the ring gear. The QCA tooth profile incorporates four circular arcs and a straight segment defined by their radii r_i $(i = t, a, d, r)$ and its length l. These circular arcs and the straight segment connect tangentially with each other from the addendum radius of the toothed element to the dedendum radius to provide a smooth transition from the top land to the root of the teeth. The straight segment and the circular arcs are organized on each tooth flank from the top land to the root as the tip circular arc r_t, the addendum circular arc r_a, the straight segment l, the dedendum circular arc r_d, and the root circular arc r_r, as shown in Fig. 9.

This tooth profile is based on the tooth profiles employed in [20] and [16]. As opposed to the tooth profile employed in [20], the QCA as proposed in [16] incorporates two additional circular arcs: the tip arc r_t to connect the top land region of the teeth to the addendum circular arc r_a; and the root circular arc r_r to connect the root region to the dedendum circular arc r_d. Those two additional arcs in the tooth profile play a fundamental role to avoid interference between the tooth profiles of the flexible spline and the ring gear once the deflection has been applied to the flexible spline by the wave generator.

The QCA tooth profile has been developed for the particular meshing characteristics of SWG drives

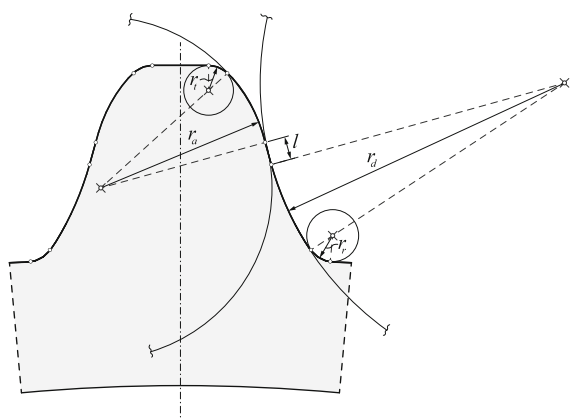

Fig. 9 Gear tooth using the QCA tooth profile

where a tooth of the flexible spline enters a tooth slot of the ring gear by sliding on one of its flanks to then exit the slot by sliding on the other flank [16]. The use of the QCA profile with smooth transitions to the top land and the root regions of the teeth of both the flexible spline and the ring gear proves advantageous in SWG drives.

3 Geometries of the wave generator

Several geometries of the wave generator have been studied and the stresses induced in the flexible spline for half a revolution of the wave generator have been obtained and compared. These wave generator geometries are:

1. *Elliptical* Based on the traditional wave generator as proposed by Musser [1].
2. *Simplified* Based on two rolling elements as proposed by Kosse [15].
3. *Four roller* Based on four rolling elements as proposed by Carlson Robinson [17].
4. *Parabolic* As proposed in this work (see below).

There are two main parameters that limit and influence the dimensions of the wave generator. These are the total deflection d to be imposed on the flexible spline and the undeformed inner radius of the flexible spline r_{fs}. The deflection d is defined as

$$d = m(N_{\mathrm{rg}} - N_{\mathrm{fs}}) \tag{1}$$

where m is the module of the toothed elements of the drive and N_i ($i = \mathrm{rg}, \mathrm{fs}$) represents number of teeth of the ring gear ($i = \mathrm{rg}$) and the flexible spline ($i = \mathrm{fs}$), respectively. Once applied, the deflection d makes the flexible spline pitch circle to deflect and coincide with the pitch circle of the ring gear in the areas around the major axis or lobes of the wave generator. Half of the deflection d constitutes the height of the strain wave that the wave generator imposes on the flexible spline [1].

The undeformed inner radius of the flexible spline r_{fs} can be determined by

$$r_{\mathrm{fs}} = \frac{N_{\mathrm{fs}} m}{2} - h_d m - t_r \tag{2}$$

where N_{fs} is the number of teeth of the flexible spline, h_d is the dedendum coefficient of the teeth of the flexible spline, and t_r is the rim thickness of the flexible spline. The critical regions of the wave generator are the lobes or major axis regions. These regions impose the deflection d on the flexible spline and are computed as a function of both the deflection d and the undeformed inner radius of the flexible spline r_{fs}.

3.1 Elliptical wave generator

The elliptical wave generator geometry is defined similarly to the one proposed by Musser in 1959 [1]. Figure 10 shows the elliptical wave generator in its coordinate system S_{wg} with reference node $\mathrm{RP}_{\mathrm{wg}}$ located on its center.

The major axis of the elliptical wave generator is determined by

$$a = r_{\mathrm{fs}} + \frac{d}{2} \tag{3}$$

where a is the semi-length of the major axis of the ellipse, r_{fs} is the undeformed inner radius of the flexible spline, and d is the deflection to be applied to the flexible spline as defined above. The semi-length of the minor axis b is defined by subtracting half of the deflection to the undeformed inner radius of the flexible spline,

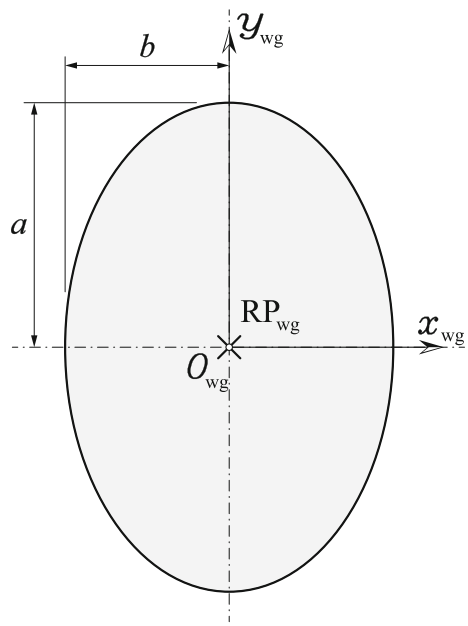

Fig. 10 Elliptical wave generator

$$b = C\left(r_{\text{fs}} - \frac{d}{2}\right) \tag{4}$$

Here, C is defined as the minor axis reduction coefficient, a user defined coefficient that can be equal or smaller than 1.0. This coefficient allows the semi-length of the minor axis b to be shorter than its maximum theoretical value and will be the subject of investigation in this work in order to determine the improved geometry for this type of wave generator.

3.2 Simplified wave generator

The simplified wave generator geometry refers to a geometry consisting of two semicircles and two straight sections with a reference node RP_{wg} on its center, as shown in Fig. 11. The straight sections connect both semicircles parallel to the vertical axis y_{wg}. The radius of the semicircles r_{pp} must be smaller than the undeformed inner radius of the flexible spline r_{fs}. This radius r_{pp} is also the radius of the circular pushing pins that this wave generator employs to deflect the flexible spline into meshing. The dimension l_{wg} of the wave generator is equal to the semi-length of the major axis a of the elliptical wave generator geometry as defined in Eq. (3).

The radius of the pushing pins r_{pp} is obtained with the following formula which relates this radius with the undeformed inner radius of the flexible spline r_{fs},

$$r_{\text{pp}} = C\left(r_{\text{fs}} - \frac{d}{2}\right) \tag{5}$$

where C is the minor axis reduction coefficient as previously defined. This ensures that the maximum radius of the pushing pins r_{pp} is equal to the minimum inside radius of the flexible spline after being deflected, which is equal to the inner radius of the flexible spline r_{fs} minus half the deflection d. This creates some clearance inside the undeformed flexible spline for the pushing pins to be inserted before applying the deflection d and deforming the flexible spline inward along the shorter dimension of the simplified wave generator. The simplified wave generator deflects the flexible spline outward along the dimension l_{wg} of the simplified wave generator.

3.3 Four roller wave generator

Figure 12 shows the definition of the four roller wave generator based on [8, 13, 17]. In this figure, a is the

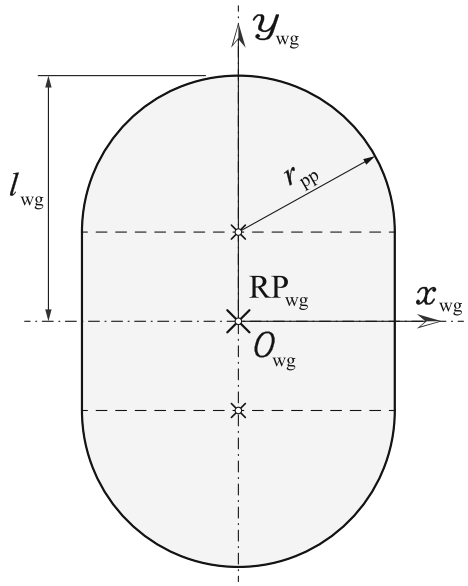

Fig. 11 Simplified wave generator

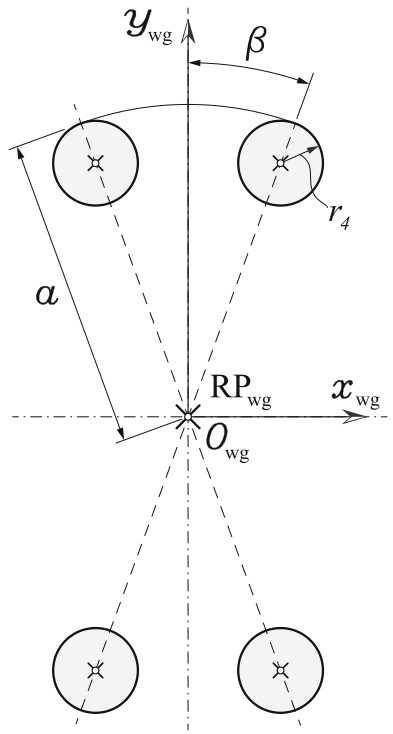

Fig. 12 Four roller wave generator

semi-length of the major axis of the elliptical wave generator as previously defined in Eq. (3), r_4 is the radius of the rollers, and β is the aperture angle of each roller from the vertical axis y_{wg}. It can be seen that the four roller wave generator geometry deflects into meshing the inner diameter of the flexible spline along the whole angle β in both the top and bottom regions of the major axis of the wave generator.

This wave generator geometry was aimed to ensure that a large number of teeth of the flexible spline will be in mesh with the ring gear, further increasing the load transmission capability of the drive [17]. However, the obtained results shown in the following section will advise against its application in SWG drives.

3.4 Parabolic wave generator

The parabolic wave generator makes use of a parabola as the portion of the geometry of the wave generator that makes contact with the inner diameter of the flexible spline or lobes of the wave generator. It consists of two parabolic regions on the top and bottom sections of the wave generator connected by means of three circular arcs on each side and a reference node RP_{wg} on its center, as shown in Fig. 13.

The three connecting circular arcs on each side are two connector arcs and a lateral arc. The connector arcs are tangent to both their adjacent parabolic region and the lateral arc. In Fig. 13, O_c and O_l represent the centers of the connector arcs and the lateral arc, respectively, on the right side of the parabolic wave generator. The semi-lengths a and b of the minor and major axes of the wave generator, respectively, are computed similarly to those of the elliptical wave generator geometry with Eqs. (3) and (4).

The points of the parabolic region are defined in the coordinate system of the wave generator S_{wg} as follows,

$$\mathbf{r}_p = \begin{bmatrix} x \\ a - a_p x^2 \\ 0 \\ 1 \end{bmatrix} \tag{6}$$

where a_p is the parabola coefficient and x is the abscissa coordinate of each point. The parabola coefficient a_p is a user-defined parameter that is proportional to the curvature of the parabolic region.

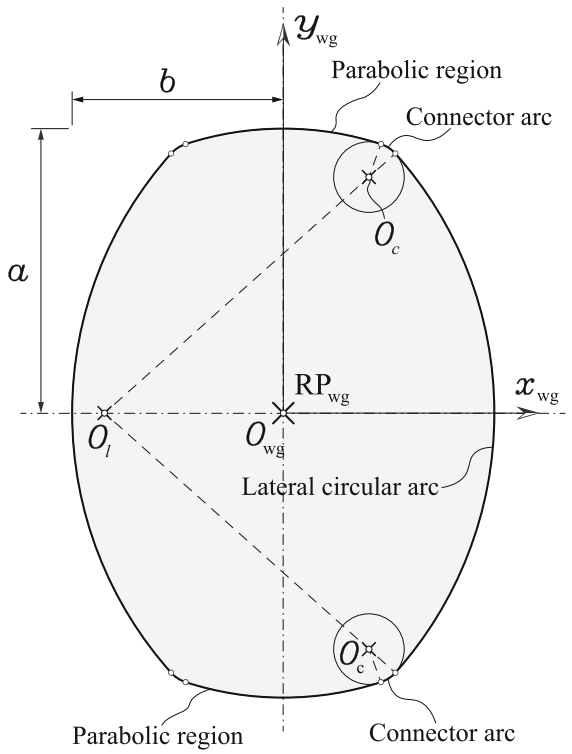

Fig. 13 Parabolic wave generator

The use of the semi-length of the major axis a in this formula makes the center and topmost point of the parabolic region equal to that of the elliptical wave generator.

Component x of the parabolic region, however, is limited between $-C_p b$ and $C_p b$, where C_p is defined as the parabola length reduction coefficient, a user-defined parameter that must be equal or smaller than 1.0. On the other hand, b is equal to the semi-length of the minor axis of the elliptical wave generator as previously defined in Eq. (4). Finally, the radii of the connector arcs r_c are also specified to transition to the lateral circular arcs of the parabolic wave generator.

The centers of the lateral arcs of the parabolic wave generator are located along the minor axis of the elliptical wave generator as defined above. In order to obtain the radius of the lateral arcs, a non-linear equation is solved guaranteeing that the connector arc of specified radius r_c is tangent to both the parabolic region and the lateral arcs of the parabolic wave generator.

4 Numerical examples

This section focuses on the determination of improved geometries of the wave generator to enhance the mechanical performance of SWG drives. The reference design parameters of the reference SWG drive are shown in Table 2. The quadruple circular arc (QCA) tooth profile has been applied to the teeth of the flexible spline and the ring gear. The layout used for the analyses considers the wave generator as the input member and the flexible spline as the output member of the drive. The ring gear is fixed, as shown in Fig. 2a. The flexible spline of the reference SWG drive case has 120 teeth and the ring gear has 122 teeth. This leads to a gear reduction ratio m_G of -60 for the considered layout which is computed with the following equation,

$$m_G = \frac{N_D}{N_D - N_F} \tag{7}$$

where N represents number of teeth and subscripts D and F indicate the driven (flexible spline) and fixed element (ring gear) of the drive, respectively [1]. Therefore, when the wave generator rotates 60 revolutions in a particular direction of rotation, the flexible spline performs one rotation in the opposite direction while the ring gear is fixed. With the given parameters, the to-be-imposed deflection d on the flexible spline is equal to 2 mm while the undeformed inner radius of the flexible spline r_{fs} is equal to 58.2 mm. For this reason, the semi-length of the major axis a or dimension l_{wg} of the simplified wave generator is equal to 59.2 mm as determined by Eq. (3) and shown in Table 2.

Steel is selected for the flexible spline and the ring gear elements of the drive, with modulus of elasticity $E = 210$ GPa and Poisson's ratio $v = 0.29$, as shown in Table 2. An output torque of 20 Nm is considered at the flexible spline. The wave generator and the pushing pins are modeled as rigid elements, which means that their mechanical properties do not need to be considered in the model [18].

The values of the maximum tensile and compressive stresses on SWG drives vary significantly at different regions of the flexible spline. In order to have a common value indicator of the state of the stress for the purpose of evaluation of their mechanical performance, the maximum von Mises equivalent stress is obtained and its variation shown over the process of meshing for half revolution of the wave generator.

4.1 Elliptical wave generator

Figure 14 shows the variation of the maximum von Mises stress on the flexible spline throughout half revolution of the elliptical wave generator with minor axis reduction coefficient C varying between 0.975 and 1.000. The maximum von Mises stress for the

Table 2 Parameters of design of the reference SWG drive

Parameter	Flexible spline	Ring gear	[units]
Number of teeth, N	120	122	–
Module, m	1		mm
Pressure angle, α	20		deg
Addendum coef., h_a	0.6		–
Dedendum coef., h_d	0.8		–
Face width, F_w	10		mm
Rim thickness, t_r	1	2	mm
Semi-length of major axis, l_{wg} or a	59.2		mm
Radius of tip circular arc, r_t	0.3		mm
Radius of addendum circular arc, r_a	1.0		mm
Length of straight segment, l	0.2		mm
Radius of dedendum circular arc, r_d	2.0		mm
Radius of root circular arc, r_r	0.3		mm
Modulus of elasticity, E	210		GPa
Poisson's ratio, v	0.29		–
Output torque, T	20	–	Nm

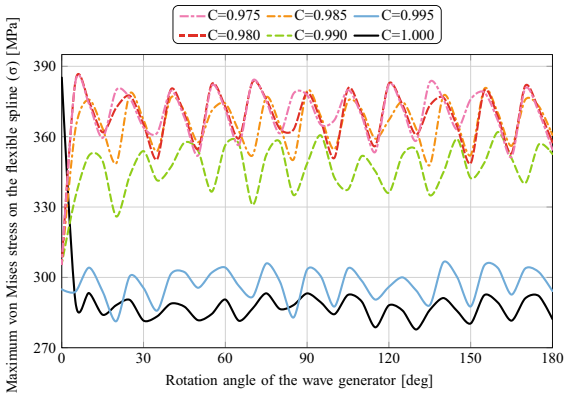

Fig. 14 Variation of the maximum von Mises stress on the flexible spline for different elliptical wave generator geometries

cases where the minor axis reduction coefficient C is between 0.975 to 0.985 are comparable. When the minor axis reduction coefficient C increases to 0.990, the maximum von Mises stress reduces slightly. Further increment of the minor axis reduction coefficient C to take the value of 0.995 causes a reduction of the maximum von Mises stress and its oscillating tendency gets slightly reduced, as shown in Fig. 14. The oscillatory behavior is caused by the engagement and disengagement of different pairs of teeth while the wave generator rotates.

When the minor axis reduction coefficient C increases to 1.000, the variation of maximum von Mises stress reaches its lowest value, as shown in Fig. 14. For this value of the minor axis reduction coefficient C, there is an initial peak of maximum von Mises stress of 385.15 MPa which is caused by the initial deflection on the flexible spline produced by this relatively large wave generator. This initial peak of maximum von Mises stress reduces once the torque is fully applied and the rotation of the wave generator begins. Consequently, the improved geometry of the elliptical wave generator considers a minor axis reduction coefficient C equal to 1.0.

Figure 15 shows the variations of maximum tensile, absolute compressive, and equivalent von Mises stresses on the flexible spline throughout half revolution of the elliptical wave generator using a minor axis reduction coefficient C of 1.0. For this case, the maximum tensile stress is considerably larger than the absolute maximum compressive stress and yields an average value of 295.763 MPa for half revolution of the wave generator.

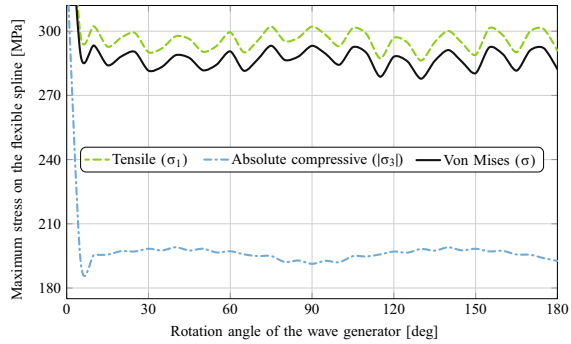

Fig. 15 Variation of the maximum tensile, maximum absolute compressive and von Mises stresses on the flexible spline when an elliptical wave generator with minor axis reduction coefficient $C = 1.0$ is applied

4.1.1 *Location of stresses*

Figures 16 and 17 show the distributions of tensile (σ_1) and compressive (σ_3) stresses once the elliptical

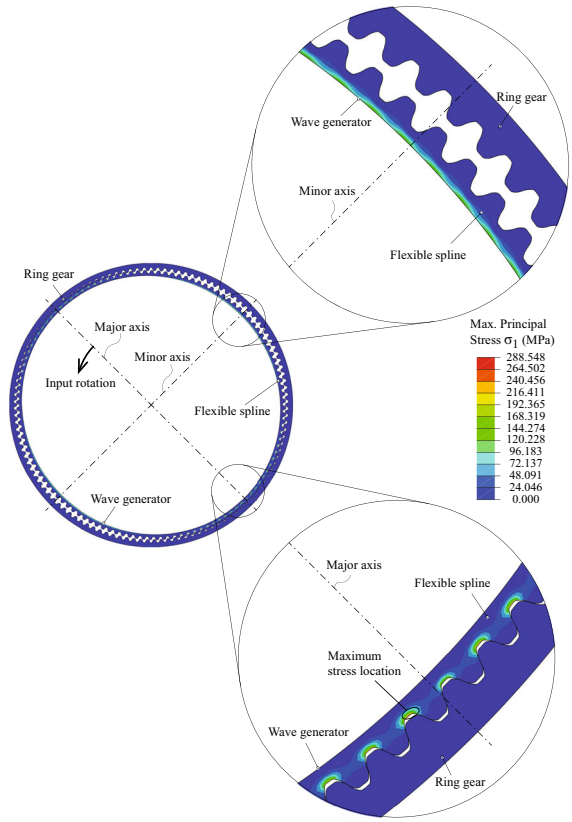

Fig. 16 Distribution of tensile stresses around the major and minor axes regions of the SWG drive when an elliptical wave generator with minor axis reduction coefficient $C = 1.0$ is applied

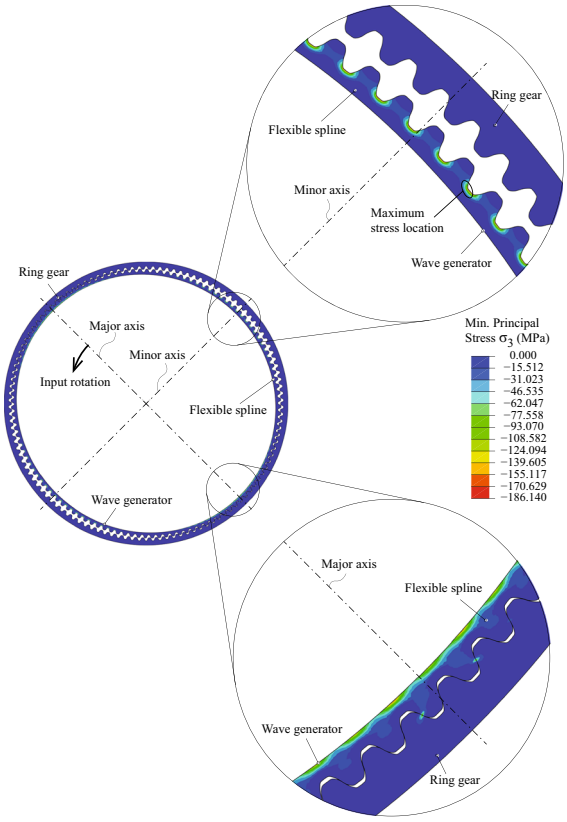

Fig. 17 Distribution of compressive stresses around the major and minor axes regions of the SWG drive when an elliptical wave generator with minor axis reduction coefficient $C = 1.0$ is applied

wave generator has rotated counterclockwise 45 degrees. Included are details of the minor and major axes regions of the drive. Tensile stress is experienced by the flexible spline on the root area of its teeth near the major axis of the drive while near the minor axis, the tensile stress is concentrated on the inner diameter of the flexible spline due to its inward deflection. The maximum tensile stress is located on the root area of the flexible spline close to the major axis of the wave generator.

On the other hand, compressive stress is concentrated on the inner diameter of the flexible spline near the major axis of the drive due to the continuously imposed deflection by the wave generator in this area. Near the minor axis, however, compressive stress is experienced at the root region of the flexible spline, as shown in Fig. 17. The compressive stress experienced by the flexible spline and the ring gear due to the tooth-to-tooth contact is remarkably smaller than that occurring on the inner diameter of the flexible spline. Similarly to the tensile stress, the maximum compressive stress is found on the root of a tooth of the flexible spline but near the minor axis in this case.

These distributions of stress are similarly obtained for any geometry of the wave generator. In SWG drives, the compressive stress concentrates on the inner diameter of the flexible spline and the tensile stress on the root area of the teeth of the flexible spline near the lobes of the wave generator. This is opposite near the minor axis of the drive where the compressive stress concentrates on the root area of the flexible spline and the tensile stress on the inner diameter of the flexible spline. Figure 18 shows the distribution of von Mises (σ) stresses on the SWG drive after the wave generator has rotated 45 degrees counterclockwise. Similarly to the distribution of tensile stress in Fig. 16, the maximum von Mises stress is located on the root region of the flexible spline near the major

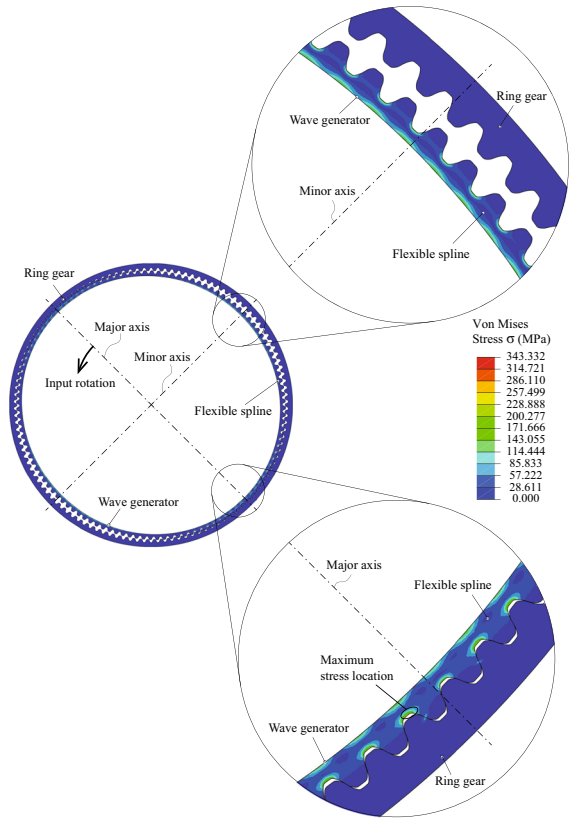

Fig. 18 Distribution of von Mises stresses around the major and minor axes regions of the SWG drive when an elliptical wave generator with minor axis reduction coefficient $C = 1.0$ is applied

axis of the wave generator. This is caused by the larger tensile stress as compared to the compressive stress which dominates the von Mises stress as an equivalent of the stresses experienced in SWG drives.

4.2 Simplified wave generator

Figure 19 shows the variation of the maximum equivalent von Mises stress on the flexible spline throughout half revolution of the simplified wave generator geometry with minor axis reduction coefficient C varying between 0.93 and 0.98. The maximum von Mises stress for the cases where the minor axis reduction coefficient C is equal to 0.93 and 0.94 are comparable. When the minor axis reduction coefficient C increases to 0.95, the variation of maximum von Mises stress reduces slightly. For a minor axis reduction coefficient C of 0.96, the variation of maximum von Mises stress reduces further as shown in Fig. 19. When the minor axis reduction coefficient C increases to 0.97, the variation of the maximum von Mises stress reaches the lowest values. However, further increasing the minor axis reduction coefficient C to 0.98 results on a surge of the maximum von Mises stress and limits the maximum value of the minor axis reduction coefficient for this study.

The simplified wave generator geometry having a minor axis reduction coefficient C equal to 0.97 is being selected as the improved simplified wave generator geometry because it yields the lowest maximum von Mises stress. Figure 20 shows the variations of maximum tensile, absolute maximum compressive, and maximum von Mises stresses on the flexible spline throughout half revolution of the wave generation using the improved simplified wave generator geometry.

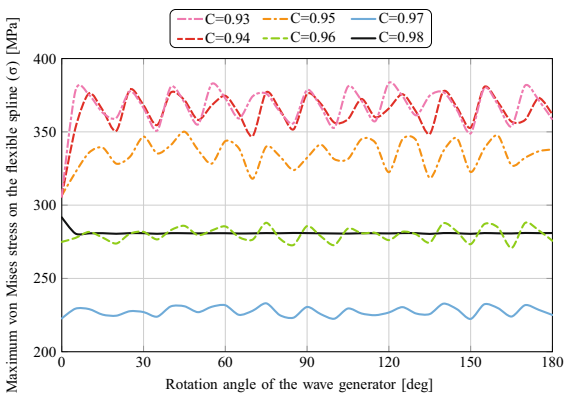

Fig. 19 Variation of the maximum von Mises stress on the flexible spline with different simplified wave generator geometries

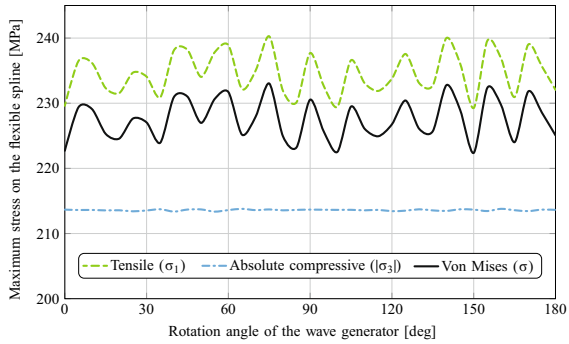

Fig. 20 Variation of the maximum tensile, maximum absolute compressive and von Mises stresses on the flexible spline when a simplified wave generator geometry with minor axis reduction coefficient $C = 0.97$ is applied

4.3 Four roller wave generator

After performing several finite element analyses with the four roller wave generator geometry modifying the aperture angle β and keeping the radius of the roller r_4 constant and equal to 8 mm, it is observed that the aperture angle β significantly influences the stresses on the flexible spline. Since a radius of the roller r_4 equal to 8 mm provides significant clearance for the aperture angle β equal to 10 degrees, this value is selected as the minimum aperture angle for the analyses.

On the other hand, after performing several analyses keeping the aperture angle β constant and varying the radius of the roller r_4, it is concluded that the radius of the roller r_4 does not constitute an influential parameter towards improving the mechanical performance of SWG drives with the four roller wave generator geometry. Different values of the radius of the roller r_4 lead to similar stress results on the flexible spline while keeping the aperture angle β constant.

Figure 21 shows the variation of the maximum von Mises stress experienced by the flexible spline for values of the aperture angle β between 10 and 20 degrees. The maximum stress experienced by the flexible spline considerably rises with higher values of the aperture angle β which is caused by the considerably open four rollers imposing deflection on the inner diameter of the flexible spline at all times and at four locations.

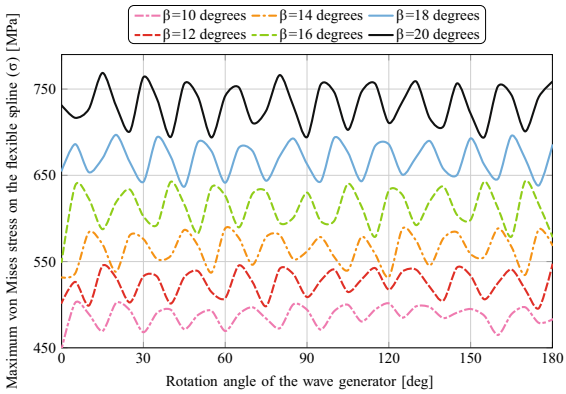

Fig. 21 Variation of the maximum von Mises stress on the flexible spline with for roller wave generator and different values of the aperture angle β

Figure 22 shows the variations of maximum tensile, absolute compressive, and von Mises stresses experienced by the flexible spline throughout half revolution of the wave generator using the four roller wave generator of 10 degrees of aperture angle β and 8 mm of radius of the roller r_4. The average maximum tensile stress is 502.806 MPa. This is considerably higher than the average maximum tensile stress obtained with the improved simplified and elliptical wave generator geometries.

With the four roller wave generator, the maximum absolute compressive stress shows an average value of 290.984 MPa. This variation of maximum absolute compressive stress shows a reduced oscillatory behavior as compared to the variations of maximum tensile and von Mises stresses. The average value of maximum von Mises stress is 487.764 MPa.

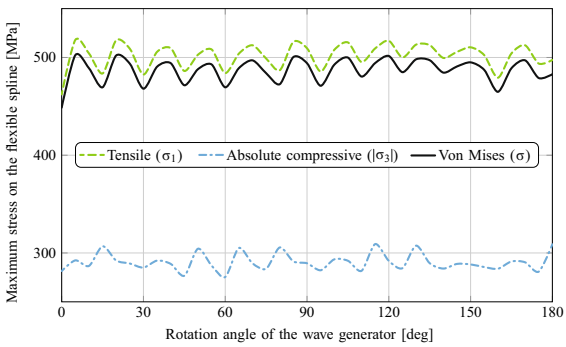

Fig. 22 Variation of the maximum tensile, maximum absolute compressive and von Mises stresses on the flexible spline when the four roller wave generator is applied

For both variations of maximum tensile and von Mises stresses, the results show certain oscillatory behavior caused by the engagement and disengagement of different pairs of teeth in contact, which share the transmitted load between the flexible spline and the ring gear while the wave generator rotates. However, the initial value of maximum tensile and von Mises stresses is slightly lower than the later developed after the torque is applied. The initial value of maximum absolute compressive stress on the flexible spline is similar to the later developed throughout a half revolution of the wave generator.

With the four roller wave generator geometry, the aperture angle β should be reduced to the lowest possible value while keeping the rollers clear from contacting one another using the radius of the roller r_4. Even though a minimum variation of maximum von Mises stress is found as a function of the aperture angle β, this variation of maximum stress is still considerably larger than any previously obtained variation of stress with the improved geometries of the simplified and elliptical type wave generator.

These stress results deem the four roller wave generator unsuitable for enhancing the mechanical performance of SWG drives. Four rollers in contact with the inner diameter of the flexible spline lead to much larger stresses than having only two lobes, as in the other geometries of the wave generator. Besides, the lack of a large contact area between the wave generator and the inner diameter of the flexible spline leads to large concentration of stresses.

4.4 Parabolic wave generator

After performing several analyses studying the influence of the minor axis reduction coefficient C with the parabolic wave generator, it is observed that the stresses on the flexible spline do not significantly vary as a function of this parameter. For this reason, the minor axis reduction coefficient C is selected equal to 1.0 for further analyses of SWG drives with the parabolic wave generator geometry. The parabola coefficient a_p critically influences the geometry of the parabolic wave generator and the stresses obtained in SWG drives. Figure 23 shows a detail of parabolic regions with values of the parabola coefficient a_p equal to 0.005, 0.007, 0.009, and 0.010 1/mm. With the employed parameters shown in Table 2, the semi-

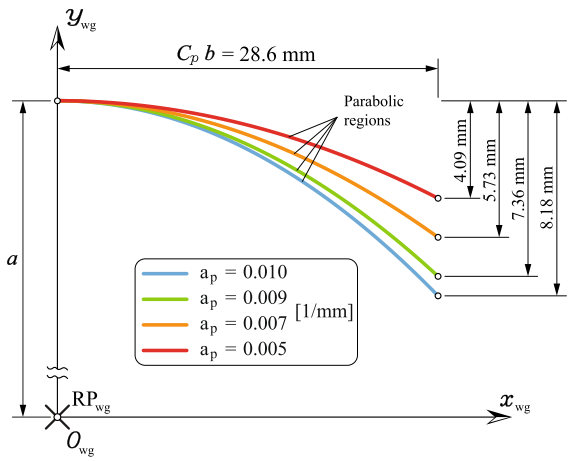

Fig. 23 Geometry of the parabolic region of the parabolic wave generator for different values of the parabola coefficient a_p

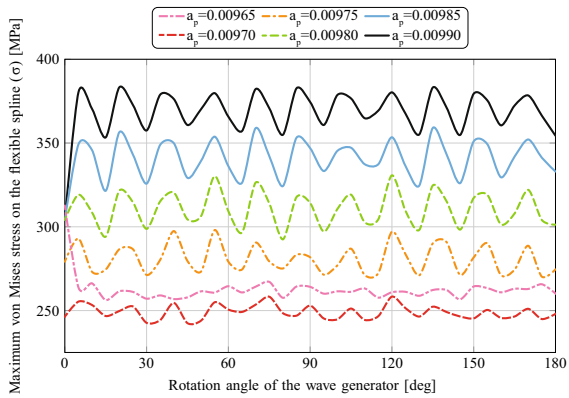

Fig. 24 Variation of the maximum von Mises stress on the flexible spline with different values of the parabola coefficient a_p applied to the wave generator geometry

length of the major axis a of the wave generator is equal to 59.2 mm while the semi-length of the minor axis b is equal to 57.2 mm where the parabolic region extends in the horizontal direction up until a value equal to the parabola length reduction coefficient C_p times the semi-length of the minor axis b. With the parabola length reduction coefficient C_p equal to 0.5, the parabolic regions extend 28.6 mm on the horizontal direction. However, modifying the parabola coefficient a_p changes the vertical location of the last point of the parabolic region, as shown in Fig. 23. The influence of the parabola coefficient a_p on the geometry of the parabolic region approximately accounts for less than 1 mm change on the vertical location of the last point for a change of 0.001 1/mm on the parabola coefficient a_p.

After performing several analyses with different values of the parabola coefficient a_p while keeping the remaining parameters constant, it has been observed that parabola coefficients a_p lower than 0.00965 1/mm lead to remarkably high stresses, rendering this range of the parabola coefficient a_p ineffective to improve the mechanical performance of SWG drives with the considered parameters. On the other hand, when using parabola coefficients a_p equal or higher than 0.00990 1/mm, the resulting stresses are the same. For these reasons, the results shown are for parabola coefficients a_p between 0.00965 and 0.00990 1/mm in increments of 0.00005 1/mm, while the parabola length reduction coefficient C_p and the radius of the connector arc r_c are selected equal to 0.5 and 10 mm, respectively.

Figure 24 shows the variation of maximum von Mises stress on the flexible spline throughout half revolution of the parabolic wave generator for different values of the parabola coefficient a_p. As the parabola coefficient a_p increases, the variations of maximum von Mises stress reduce until reaching the lowest variation of maximum von Mises stress when the parabola coefficient a_p equals 0.00970. Further increasing the parabola coefficient a_p leads to higher variations of maximum von Mises stress. The maximum variation of von Mises stress is obtained when the parabola coefficient a_p is equal to 0.00990 1/mm, when the results are approximately the same for equal or higher values of the parabola coefficient a_p.

The oscillatory behavior of the variation of maximum von Mises stress shown in Fig. 24 reduces slightly with parabola coefficients a_p equal to 0.00965 and 0.00970 1/mm. For values of the parabola coefficient a_p between 0.00980 and 0.00990 1/mm, the initial maximum von Mises stress values coincide before the application of torque to then diverge after its application. Consequently, middle range values of the parabola coefficient a_p are recommended for improved performance of SWG drives. Here, the parabolic wave generator with parabola coefficient a_p equal to 0.0097 1/mm is selected as the improved parabolic wave generator geometry as a function of the parabola coefficient a_p.

Several analyses have been performed varying the parabola length reduction coefficient C_p along its entire range, showing that parabola length reduction coefficients C_p equal or lower than 0.42 lead to similar

stress results. On the other hand, when using parabola length reduction coefficients C_p equal or higher than 0.52, the obtained stresses increase remarkably. For these reasons, the results are shown for values of the parabola length reduction coefficient C_p between 0.42 and 0.52. Figure 25 shows the variation of maximum von Mises stress on the flexible spline throughout the simulation of meshing for different values of the parabola length reduction coefficient C_p. Between parabola length reduction coefficients C_p equal to 0.42 and 0.51, the maximum von Mises stress reduces, where the variation of maximum von Mises stress experienced by the flexible spline reaches its lowest value with parabola length reduction coefficient C_p equal to 0.51. This is caused by the enlargement of the parabolic region of the wave generator in contact with the inner diameter of the flexible spline. However, when the parabola length reduction coefficient C_p is increased to values equal to 0.52 or higher, the maximum von Mises stress experienced by the flexible spline increases considerably beyond the maximum stress values obtained before.

For low values of the parabola length reduction coefficient C_p, the initial values of the maximum von Mises stress coincide before the application of torque. However, when the parabola length reduction coefficient C_p is equal to 0.48 and 0.50, the initial value of maximum von Mises stress is similar to the later developed through the process of meshing. For values of the parabola length reduction coefficient C_p equal or higher than 0.51, the initial maximum von Mises stress is higher than the average value of the variation of maximum von Mises stress experienced by the flexible spline. This is caused by the relatively large parabolic region of the wave generator in contact with the inner diameter of the flexible spline.

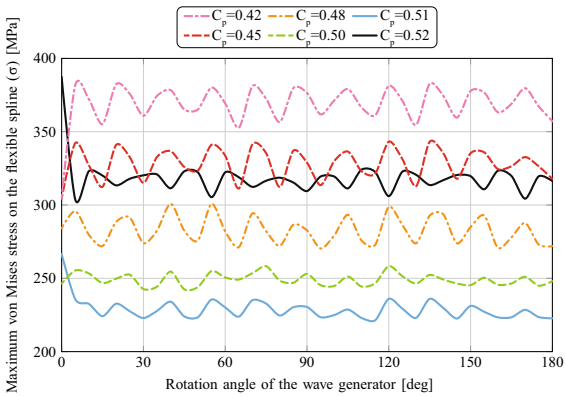

Fig. 25 Variation of the maximum von Mises stress on the flexible spline with different values of the parabola length reduction coefficient C_p applied to the wave generator geometry

The parabolic wave generator with parabola length reduction coefficient C_p equal to 0.51 is selected as the improved parabolic wave generator geometry as a function of the parabola length reduction coefficient C_p because it leads to the lowest variation of maximum von Mises stress on the flexible spline throughout the simulation of meshing of half a revolution of the wave generator.

Several analyses have been performed modifying the radius of the connector arc r_c while using the obtained values of the parabola coefficient a_p and the parabola length reduction coefficient C_p where higher values of the radius of the connector arc r_c lead to higher stresses. For this reason, there is no improved geometry of the parabolic wave generator based on the radius of the connector arc r_c. This is also due to the larger influence on stresses provided by the parabola coefficient a_p and the parabola length reduction coefficient C_p. These parameters provide the final geometry of the parabolic region of this type of wave generator which is in contact and deflecting the inner diameter of the flexible spline at all times. The parabolic region constitutes the critical region for mechanical performance of SWG drives employing this type of wave generator.

Table 3 shows the improved values of the parameters used to define the geometry of the parabolic wave generator. These improved values have been found by varying each parameter and evaluating their influence over stresses. They have been found for SWG drives of parameters shown in Table 2.

Figure 26 shows the variations of maximum tensile, absolute compressive, and von Mises stresses on

Table 3 Parameters of the improved geometry of the parabolic wave generator.

Parameter	[units]	
Minor axis reduction coef., C	–	1.0
Parabola coef., a_p	1/mm	0.0097
Parabola length reduction coef., C_p	–	0.51
Radius of the connector arc, r_c	mm	10.0

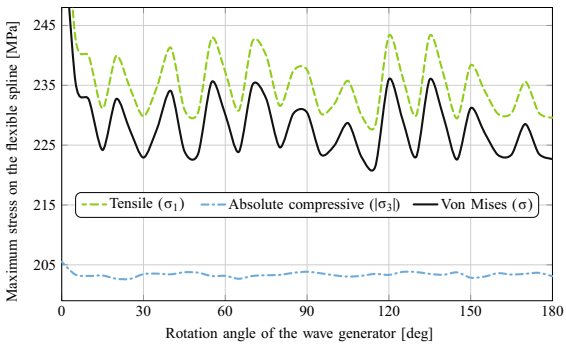

Fig. 26 Variation of the maximum tensile, maximum absolute compressive and von Mises stresses on the flexible spline when the parabolic wave generator is applied

the flexible spline with the parabolic wave generator of parameters shown in Table 3. Although not shown in the figure, the initial peaks of maximum tensile and von Mises stresses are equal to 274.800 and 266.610 MPa, respectively.

The variations of maximum tensile and von Mises stresses in Fig. 26 show a considerable large oscillatory behavior. However, the variation of the absolute maximum compressive stress shows a smooth variation due to the constant contact between the lobes of the wave generator and the inner diameter of the flexible spline.

The performed study and variation of the parameters of the parabolic wave generator aiming to reduce the obtained stresses lead to a remarkably improved geometry of the parabolic wave generator for this SWG drive design. The improved geometry of the parabolic wave generator provides a smoother contact between its parabolic regions, or lobes of the wave generator, and the inner diameter of the flexible spline.

4.5 Comparison of results obtained with different geometries of the wave generator

The improved geometries found for each type of wave generator are summarized as follows:

- *Simplified* minor axis reduction coefficient C equal to 0.97.
- *Elliptical* minor axis reduction coefficient C equal to 1.0.
- *Four roller* aperture angle β and radius of the roller r_4 equal to 10 degrees and 8 mm, respectively.
- *Parabolic* parameters shown in Table 3.

These results were obtained for the SWG drive design of parameters shown in Table 2 and lead to the lowest maximum von Mises stress on the flexible spline, a critical element towards the improvement of the mechanical performance of SWG drives.

Table 4 shows the average values of maximum tensile, absolute compressive, and von Mises stresses on the flexible spline obtained by finite element analysis of SWG drives. These stresses occur in the flexible spline when each improved geometry of the wave generator is applied. The lowest average maximum von Mises stress of a value approximately equal to 228 MPa is obtained with the simplified and parabolic wave generator geometries. However, while their resulting average maximum tensile stress is also similar, the results obtained with these wave generator geometries differ in their average absolute maximum compressive stress by approximately 10 MPa, where the lower average maximum compressive stress is found with the parabolic wave generator geometry.

On the other hand, the elliptical wave generator geometry leads to larger average maximum tensile and von Mises stresses than the simplified and parabolic wave generator geometries. These average maximum stresses are approximately 60 MPa higher, as shown in Table 4. However, the elliptical wave generator provides the lowest average maximum absolute compressive stress.

The four roller wave generator geometry results in considerably higher maximum stresses than any other wave generator geometry with respect to the maximum tensile, absolute compressive, and von Mises stresses.

In order to enhance the mechanical performance of SWG drives, the use of the simplified or the parabolic wave generator geometries is recommended for SWG drive designs of parameters shown in Table 2. The differences between the simplified and the parabolic wave generator geometries consist of the more complex definition of the parabolic wave generator requiring four parameters, as opposed to a single parameter as required by the simplified wave generator. However, the simplified and parabolic wave generator geometries are comparable in terms of enhancing the mechanical performance of SWG drives.

On the other hand, if the aim is to reduce the compressive stress imposed by the lobes of the wave generator on the inner diameter of the flexible spline,

Table 4 Average maximum stress experienced by the flexible spline with improved wave generator geometries of different types.

Stress wave generator	Tensile, σ_1 (MPa)	Compressive, $\lvert\sigma_3\rvert$ (MPa)	Von Mises, σ (MPa)
Elliptical	295.763	195.891	286.981
Simplified	234.746	213.595	227.680
Four roller	502.806	290.984	487.764
Parabolic	234.993	203.340	227.939

the elliptical wave generator geometry should be selected similar to the wave generator proposed by Musser in 1959 [1]. The considerably worse mechanical performance of SWG drives employing the four roller wave generator justifies its lack of use since the concept was patented in 1968 [17].

5 Conclusions

A total of four wave generator geometries have been studied and improved with the objective of reducing the resulting stresses on the flexible spline, critical element for mechanical performance of SWG drives. Out of the studied geometries of the wave generator, three are based on previously developed concepts, while a fourth geometry was proposed in this work using a parabolic curve for the lobes of the wave generator imposing the deflection on the flexible spline.

The best mechanical performance of the SWG drive in terms of lower average values of maximum von Mises and tensile stresses was obtained using the simplified and parabolic wave generator geometries. The elliptical wave generator provides the lowest average maximum absolute compressive stress, although resulting in slightly higher maximum von Mises and tensile stresses. The worse mechanical performance was obtained with the four roller wave generator, which is not capable of achieving its aim to reduce stresses in SWG drives by increasing the number of contacting regions with the flexible spline. Consequently, either the simplified or parabolic geometries of the wave generator would be recommended for enhanced mechanical performance of SWG drives.

Acknowledgements The authors express their deep gratitude to the Gleason Corporation for establishing the Gleason Doctoral Fellowship at the Rochester Institute of Technology.

Funding This research work has not received any financial support and has been performed under the authors' interest to advance the state of the art in this field.

Compliance with ethical standards

Conflict of interest The authors declare that they have no conflict of interest.

References

1. Musser CW (1959) Strain wave gearing, US Patent, 2906143
2. Hashimoto M (1989) Robot motion control based on joint torque sensing'. In: IEEE international conference on robotics and automation, pp 256–261
3. Taghirad HD, Belanger PR (1998) Modeling and parameter identification of harmonic drive systems. J Dyn Syst Meas Control 120:439–444
4. Tjahjowidodo T, Al-Bender F, Van Brussel H (2013) Theoretical modelling and experimental identification of nonlinear torsional behaviour in harmonic drives. Mechatronics 23(5):497–504
5. Lu Y-S, Lin S-M, Hauschild M, Hirzinger G (2013) A torque-ripple compensation scheme for harmonic drive systems. Electr Eng 95:357–365
6. Kayabasi O, Erzincanli F (2007) Shape optimization of tooth profile of a flexspline for a harmonic drive by finite element modelling. Mater Des 28(2):441–447
7. Li S (2016) Diaphragm stress analysis and fatigue strength evaluation of the flex-spline, a very thin-walled spur gear used in the strain wave gearing. Mech Mach Theory 104:1–16
8. Dong H, Wang D (2009) Elastic deformation characteristic of the flexspline in harmonicdrive. In: ASME/IFToMM international conference on reconfigurable mechanisms and robots, pp 363–369
9. Chen Y, Cheng Y, Tseng J, Hsieh K (2017) Study of a harmonic drive with involute profile flexspline by two-dimensional finite element analysis. Eng Comput 34(7):2107–2130

10. Sahoo V, Maiti R (2017) Load sharing by tooth pairs in involute toothed harmonic drive with conventional wave generator cam. Meccanica 53(1–2):373–394
11. Sahoo V, Maiti R (2018) Evidence of secondary tooth contact in harmonic drive, with involute toothed gear pair, through experimental and finite element analyses of stresses in flex-gear cup. Proc Inst Mech Eng Part C J Mech Eng Sci 232(2):341–357
12. Ma J, Li C, Luo Y, Cui L (2018) Simulation of meshing characteristics of harmonic reducer and experimental verification. Adv Mech Eng 10(3):1–9
13. Pacana J, Witkowski W, Mucha J (2017) Fem analysis of stress distribution in the hermetic harmonic drive flexspline. Strength Mater 49(3):388–398
14. Wang S, Jiang G, Mei X, Zou C, Zhang X, Zhang H (2019) A rapid stress calculation method for short flexspline harmonic drive. Eng Comput 36(6):1852–1867
15. Kosse V (1997) Analytical investigation of the change in phase angle between the wave generator and the teeth meshing zone in high-torque mechanical harmonic drives. Mech Mach Theory 32(5):533–538
16. Yu Z, Ting K-L (2018) Application of finite element analysis for the strain wave gear tooth surfaces design and modification. AGMA Technical Paper 9
17. Carlson JH, Robinson HA (1970) Actuators employing preloaded wave generators, US Patent, 3496782
18. ABAQUS/Standard User's Manual. Simulia, 2019
19. Godler I, Hashimoto M, Horiuchi M, Ninomiya T (2001) Performance of gain-tuned harmonic drive torque sensor under load and speed conditions. IEEE/ASME Trans Mech 6(2):155–160
20. Chen X, Liu Y, Xing J, Lin S, Xu W (2014) The parametric design of double-circular-arc tooth profile and its influence on the functional backlash of harmonic drive. Mech Mach Theory 73:1–24